ELSEVIER

Journal of Power Sources 53 (1995) 9–21

JOURNAL OF POWER SOURCES

A theory of the grid/positive active-mass (PAM) interface and possible methods to improve PAM utilization and cycle life of lead/acid batteries

D. Pavlov

Central Laboratory of Electrochemical Power Sources, Bulgarian Academy of Sciences, Sofia 1113, Bulgaria

Received 22 September 1994; accepted 26 October 1994

Abstract

Very often, the cycle life of batteries with antimony-free positive grids operating under deep-discharge cycling is determined by the grid/PAM interface. The properties of this interface are overviewed and the technological and design parameters influencing these properties, and hence determining the cycle life of the battery, are discussed. A new parameter γ is proposed. This is defined as grams of PAM per 1 cm^2 of grid-collector surface area. It has been established that the grid/PAM interface consists of two layers, namely, a corrosion layer (CL) and a layer of the active mass that collects the current from the remaining (capacity-bearing) part of the PAM (AMCL). The technological parameters that influence the specific resistivity of both CL and AMCL, as well as the surface area of the layers through which current flows between the PAM and the collector are discussed. On the basis of the principles derived from the theory of the grid/PAM interface, batteries are produced and tested.

Keywords: Positive active mass; Cycle life; Lead/acid batteries; Interface; Grid/PAM interface

1. Introduction

The positive lead/acid battery plate consists of three structural elements; active material, corrosion layer and grid. Each of them may limit the life of the plate during battery operation at 35% utilization of the active mass.

- When the plate grid is cast from high-antimony lead alloys (6–12 wt.% Sb), the service life may reach 1500 cycles and is determined by the corrosion of the grid.
- When the life of the plate is limited by softening and shedding of the positive active mass (PAM), the battery endures only 200–300 cycles.
- Finally, when the grid is made of lead or antimony-free alloys, it is the corrosion layer that limits the capacity of the positive plate. The battery exhibits a cycle life of only 20–30 cycles. As this phenomenon occurs when the grid alloy contains no antimony, it was initially called the 'antimony-free effect' but later 'premature capacity loss' (PCL).

Capacity and cycle life are set up by the design and the technology of positive-plate production.

The cycle life of the positive plate is determined by the operational conditions of the battery. The latter are related to the coefficient of PAM utilization, the current profile during charge and discharge, the duration and distribution of the overcharge, and open-circuit periods. These conditions tend to modify the genetically determined parameters of the plate. If optimum plate design and manufacturing technology are applied to give considerable power resources, the operational parameters exert less influence on the expected cycle life. By contrast, if the design and technology are not optimized, the capacity resources of the plate are limited and, hence, the cycle life depends strongly on the conditions of operation. Optimization of plate design and manufacturing technology requires profound knowledge about the mechanism of the processes that occur during battery production and operation.

2. Structure of the grid/PAM interface

2.1. Fundamentals of the model

Why does the corrosion layer exert such a strong influence on the capacity of the positive plate? The answer to this question is illustrated in Fig. 1.

SSDI 0378-7753(94)02152-S

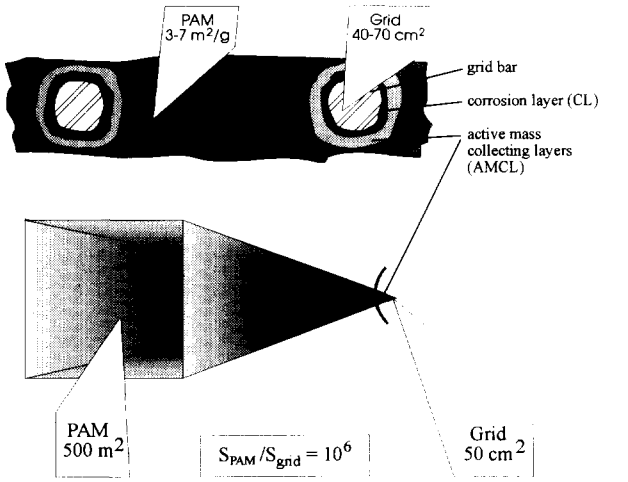

Fig. 1. Schematic representation of the relationship between the surface areas of PAM and CL. Formation of the active-mass collecting layer (AMCL). SLI plate with 100 g PAM.

The specific surface area of the lead dioxide active mass is from 3 to 8 m^2/g PAM. Assume an average value of 5 m^2/g. An SLI plate with 100 g of PAM has a surface area of about 500 m^2. The grid of such a plate has a surface area of between 40 and 70 cm^2; assume 50 cm^2. During plate discharge, the current generated on an active-mass surface of 500 m^2 is concentrated in a layer of the positive active mass and passes through a 50 cm^2 grid surface area. This results in a 10^6-fold increase in current density. It can be concluded from Fig. 1. that a layer is formed in the PAM whose basic function is to collect the current and carry it to the corrosion layer (CL). This layer can be denoted as the 'active-mass collecting layer' (AMCL). Hence, the structure of the grid/PAM interface consists of two parts: corrosion layer (CL) and active-mass collecting layer (AMCL). On the other hand, with regard to the basic function of PAM, the latter can be divided into capacity-bearing PAM and AMCL.

2.2. *Principles of positive-plate design derived from the proposed model*

On the basis of the model presented in Fig. 1, the following principles of positive-plate design can be proposed.

2.2.1. *Uniform distribution of PAM over the surface area of the grid collector*

A parameter in designing positive battery plates is the ratio, α, between the grid weight (W_{grid}) and the active-mass weight (W_{PAM}), i.e.,

$$\alpha = W_{grid}/(W_{PAM} + W_{grid}) \quad (1)$$

The value of α varies between 0.35 and 0.60; the tendency is to reduce this value by as much as possible. In view of the critical role of the grid/PAM interface under deep-cycling duty, the introduction of another parameter (γ) is necessary. This reflects the amount of active mass per cm^2 of grid surface (S_{grid}) (g PAM/cm^2 collector surface), i.e.,

$$\gamma = W_{PAM}/S_{grid} \quad (2)$$

The value of γ depends on the design of the plate. This can be demonstrated by the cross section of two plates of different design (Fig. 2).

In the first type of plate design, a plane surface (Fig. 2(a)) is covered by an active-mass layer. γ will attain a constant value throughout the surface of the collector. This will allow a current (i_d) with uniform density to pass through the grid/PAM interface. In the second type of plate design, the collector consists of grid bars that are situated asymmetrically in the plate cross section (Fig. 2(b)). The value of γ will vary along the surface of the grid bars. This will lead to a non-uniform current distribution over the grid surface. The higher the resistance of the grid/PAM interface, the greater the variation in current density on the collector surface. Thus, one of the basis principles of positive-plate design is to achieve uniform distribution of the active mass over the grid bars.

2.2.2. *Optimum value of the parameter γ*

The cycle life of the positive plate depends on:

- the coefficient of PAM utilization; this determines the intensity of the destructive processes in the positive active mass during operation
- γ parameter; this influences the processes occurring in the grid/PAM interface and increases or decreases their rates.
- conditions of operation

One analysis of the relation between the above parameters shows that there are optimum values of γ (γ_m) and the coefficient of PAM utilization η (η_m) that ensure a maximum for the cycle life of the battery (Z_m).

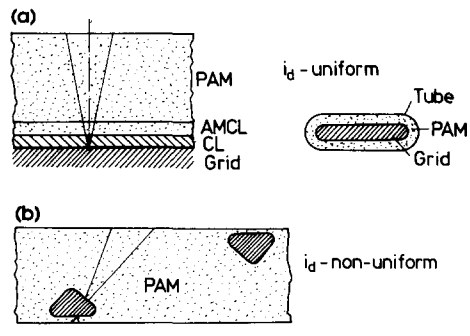

Fig. 2. Influence of the grid-bar shape and plate design on the uniformity of current distribution over the grid surface.

If $\gamma > \gamma_m$, then $\eta < \eta_m$, part of the active mass will remain unutilized and $Z < Z_m$ as the cycle life is determined by the properties of the grid/PAM interface.

If $\gamma < \gamma_m$, then $\eta > \eta_m$ and the active mass will shed from the grid. Thus, the cycle life of the positive plate will be shorter, $Z < Z_d$. A general scheme of the relationships between γ, η and Z at constant conditions of deep cycle-life testing is presented in Appendix A.

For SLI positive plates, $\gamma = 2$–2.5 g cm^{-2} and for tubular plates, $\gamma = 1.6$–1.8 g cm^{-2}, respectively. Positive plates have been designed in the author's laboratory with a 50% smaller γ value ($\gamma = 0.5$–0.8 g PAM cm^{-2}) [1] in an effort to improve PAM utilization and cycle life.

2.3. Limitation of capacity by the resistance of the grid/PAM interface

The capacity of the positive plate is equal to the sum of the electricity generated by the amount of PbO_2 in the capacity bearing PAM, i.e., $\eta_1 Q_{PAM}$, where Q is the theoretical quantity of electricity carried by PAM and η_1 is the coefficient of mass utilization, and the electricity generated by the amount of PbO_2 at the grid/PAM interface which is reduced during discharge, i.e., $\eta_2 Q_{grid/PAM}$. Thus:

$$C = \eta_1 Q_{PAM} + \eta_2 Q_{grip/PAM} \quad (3)$$

where:

$$\eta_1 Q_{PAM} \gg \eta_2 Q_{grid/PAM}$$

As the grid/PAM interface is situated on the current pathway between the PAM and the current collector, the value of $\eta_1 Q_{PAM}$ depends on the electrical conductivity of this interface.

Let it be assumed that the rate of reduction of PbO_2 at the grid/PAM interface is much smaller than that of PAM reduction. Under this condition, the interface will remain conductive during plate discharge and the capacity of the plate will be determined by Eq. (3).

If the rate of reduction of PbO_2 at the grid/PAM interface is equal to, or greater than, that of PAM reduction, then the capacity of the plate will be limited by the resistance of the above interface. i.e.,

$$C = k\eta_1 Q_{PAM} + \eta_2 Q_{grid/PAM} \quad \text{where } k < 1 \quad (4)$$

The coefficient k stands for that part of the PAM ($\eta_1 Q_{PAM}$) that is reduced during the period of sufficiently high conductivity of the grid/PAM interface.

Hollenkamp et al. [2] have measured the changes in the contact resistance (R_c) between the PAM and the grid during discharge of plates with grids cast from different alloys. The results for four types of plates are presented in Fig. 3. At the beginning of discharge, the

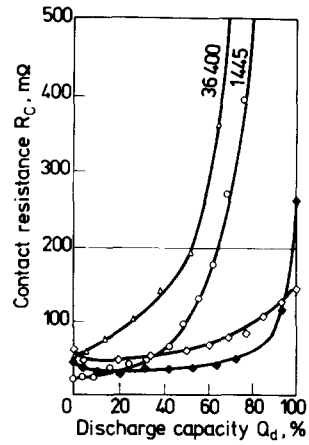

Fig. 3. Contact surface resistance (R_c) vs. % discharged capacity (100% DOD) for positive plates with grids cast from the following alloys: (△) pure Pb; (○) Pb–0.1wt.%Ca; (♦) Pb–5.3wt.%Sb; (◇) Pb–2.2wt.%Sb–0.1wt.%Sn [2].

R_c values are about 50 mΩ. An increase in the contact resistance (to 200 mΩ) limits the capacity of the plates as follows: for pure Pb down to 53%, for Pb–0.1wt.% Ca down to 63%, against 97% for Pb–5.3wt.%Sb and 100% for Pb–2.2wt.%Sb–0.1wt.%Sn plates. The electrical conductivity of the grid/PAM interface limits the capacity of plates with Pb and Pb–Ca grids, whereas the capacity of Pb–Sb and Pb–Sb–Sn plates is limited more by the properties of the PAM.

2.4. Electrical conductivity of the grid/PAM interface

The grid/PAM interface consists of a corrosion layer, the active-mass collecting layer and their interfacial boundaries. For the sake of simplicity, assume that Ohm's law describes the resistance of the grid/PAM interface. In fact, this is not quite precise as the oxides in the CL and the AMCL are semi-conductors. Furthermore, assume that the resistances of all interfaces of the layers are very small. The resistance of the CL and the AMCL is thus given by the equation:

$$R = [\rho_0 l/S]_{CL} + [\rho_0 l/S]_{AMCL} \quad (5)$$

where $\rho_{0,CL}$ and $\rho_{0,AMCL}$ are the specific resistivities of the CL and the AMCL, respectively. For electronic conductors, ρ_0 is a characteristic parameter. For semiconductors (as is the case with lead oxides), ρ_0 depends on the concentration and mobility of the major charge carriers, the concentration of dopants, and, for thin layers (as is the case with lead oxides in the CL) on the thickness of the semi-conducting layer as well. l_{CL} and l_{AMCL} are the thicknesses, and S_{CL} and S_{AMCL} the corresponding effective areas (cross sections) of CL and AMCL through which the current flows. The dependence of ρ_0, l and S of both CL and AMCL on

the technological parameters of positive plate production is outlined below.

2.5. Thermal loop at the grid/PAM interface

The specific resistivities of α-PbO_2 and β-PbO_2, along with those for Pb and Cu (for comparison) are summarized in Table 1. It can be seen that ρ_0 (α-PbO_2) = $6\rho_0$ (β-PbO_2) $\approx 500\rho_0$ (Cu). This means that α-PbO_2, though a good conductor, has a comparatively high electrical resistance.

According to Joule's law, the quantity of heat H (in calories) released by a current of I (in amps) for a time t (seconds) is given by:

$$H = 0.24I^2Rt = 0.24I^2(\rho l/S)t \quad (6)$$

It is generally accepted in technical practice that a copper wire with a cross section of 1 mm^2 is not heated if the current flowing through it does not exceed 2 A. On the basis of this value, the analogous limiting current flowing through 1 mm^2 of PbO_2 or Pb without causing it to be heated can be roughly estimated. The resulting values are presented in Table 2, along with the limiting currents for a 10 cm^2 cross section of the conductor.

If the grid/PAM interface consists of α-PbO_2 (the latter is always present in the corrosion layer) and has a surface area of 10 cm^2, the grid/PAM interface will not heat up when the current flowing through the plate is lower than 4 A. If the surface area is smaller than 10 cm^2 and the current is higher than 4 A, then the temperature at the interface rises and can reach a critical value at which the interface grid/PAM could crack. As a result of this, the area S (Eq. (6)) through which the current flows will be reduced. Consequently, the quantity of heat released with increase and hence the temperature will rise, i.e., a thermal loop is created.

Table 1
Specific resistivities of listed materials

Substance	Specific resistivity, ρ_0 (10^{-4} Ω cm)	Ref.
α-PbO_2	8.4	[3]
β-PbO_2	1.4	[3]
Pb	0.21	[4]
Cu	0.017	[4]

Table 2
Limiting current passing through a definite cross section area of a conductor without causing it to heat

Substance	Current (A/mm^2)	Current (A/10 cm^2)
α-PbO_2	0.004	4.0
β-PbO_2	0.024	24.0
Pb	0.16	160.0
Cu	2.0	2000

The grid/PAM interface contains, besides α-PbO_2, lower valency lead oxides as well, especially when the grids are made of Pb and Pb–Ca alloys. The latter have higher specific resistivity. This means that the critical current for thermal-loop initiation decreases, i.e., cracking of the CL occurs at lower currents. Inversely, if the CL is built up of β-PbO_2, a thermal loop will be initiated at higher current densities. It can be concluded therefore, that initiation of the thermal loop depends on the phase composition of the grid/PAM interface.

3. Corrosion layer

3.1. Structure of the corrosion layer and its interfaces

Fig. 4 presents micrographs of the cross section through the interface grid/corrosion layer of cycled

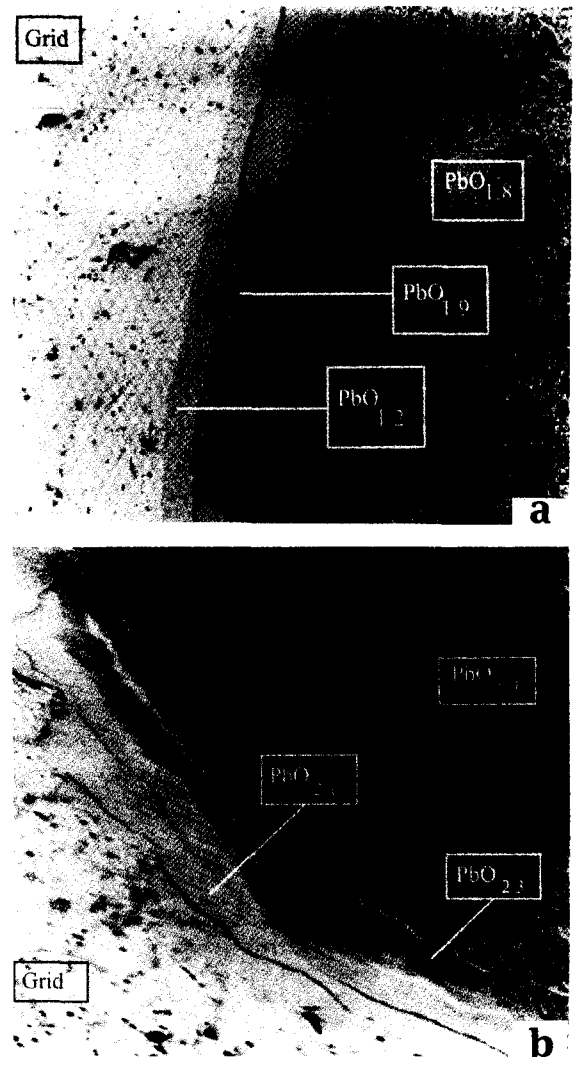

Fig. 4. Electron micrographs of a cross section through the grid/PAM interface of cycled plates in the charged state: (a) Pb–0.1wt.% Ca grids; (b) Pb–5.7wt.%Sb–0.3wt.%Sn grids [2].

positive plates with Pb–0.1wt.%Ca (Fig. 4(a)) and Pb–5.7wt.%Sb–0.3wt.%Sn (Fig. 4(b)) grids. The data have been taken from Hollenkamp et al. [2]. The CL formed on Pb–Ca grids features a layered structure. The inner sub-layer consists of $PbO_{1.2}$, and the outer is composed of $PbO_{1.8}$ and $PbO_{1.9}$ lead oxides. These layers are often separated by cracks that occupy large areas of the CL. In the case of Pb–Sb grids, the corrosion sub-layers have a dendrite structure and feature random, small cracks. The corrosion layer is composed of lead dioxide with a stoichiometric coefficient higher than 1.9. It can be seen from the above micrographs that the AMCL is different in structure for the two cases and depends on the grid alloy.

It has been established, through transmission electron microscopy and measurements of the amount of bonded water, that both PAM [5–7] and CL [8–10] consist of crystal zones with either α-PbO_2 or β-PbO_2 structures and hydrated (gel) zones. A model for the distribution of gel zones from the grid, through the CL to the PAM is presented in Fig. 5 [5]. This model takes into account the formation of cracks in the CL and at its interfaces on cycling [11–13].

The above observations indicate that the structure of the corrosion layer, its chemical composition and electrical resistivity, as well as the number and location of cracks, depend on the type and quantity of additives to the grid alloy.

3.2. Specific resistivity of the corrosion layer

The specific electronic conductivity (κ_0) is the reciprocal of the specific resistivity $\kappa_0 = 1/\rho_0$. The relationship between the electronic conductivity of lead oxides and their stoichiometric coefficient has been investigated by Lappe [14] and is presented in Fig. 6. PbO has a conductivity of $10^{-10}\ \Omega^{-1}\ cm^{-1}$. When the stoichiometric coefficient of the oxide reaches a value of 1.35, the conductivity begins to increase rapidly. For $n = 1.5$, it becomes equal to that of PbO_2.

The stoichiometric coefficient of the oxides formed in the CL depends on the electrode potential and on

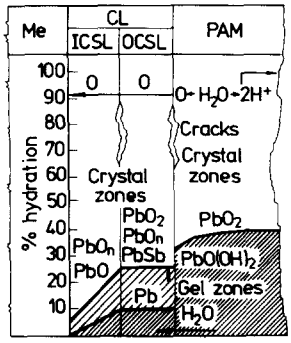

Fig. 5. Model for the distribution of gel zones in CL and PAM [5].

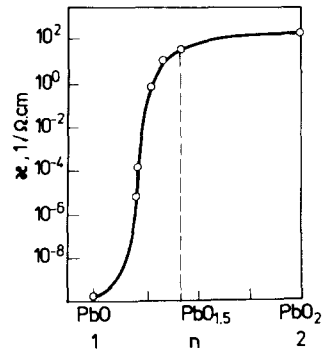

Fig. 6. Dependence of the specific electronic conductivity of lead oxides on their stoichiometric coefficient [11].

the type and amount of alloying additives that are used. The potential determines the type and rate of the reactions taking place at the electrode. These reactions include:

- reactions of oxidation of lead in the grid alloy by oxygen diffusing through the CL:

$$Pb + O \xrightarrow{v_1} PbO \tag{7}$$

$$PbO + (1-n)O \xrightarrow{v_2} PbO_n \qquad (1<n<2) \tag{8}$$

$$PbO_n + (2-n)O \xrightarrow{v_3} PbO_2 \tag{9}$$

Depending on the ratio between the rates of reactions (7)–(9), corrosion layers with various stoichiometric coefficients can be formed. If $v_1 > v_2$, a low-valency lead oxide will be obtained and the CL will exhibit high specific resistivity. If $v_1 < v_2, v_3$, the reverse situation is observed. The relationship between the conductivity of lead oxide semiconductors and their stoichiometry is outlined in Appendix B.

- self-discharge reaction between Pb and PbO_2:

$$Pb + PbO_2 \xrightarrow{v_4} 2PbO \tag{10}$$

This reaction leads to a decrease in the overall stoichiometric coefficient of the oxide in the CL and to an increase in its specific resistivity.

Alloying additives can influence the conductivity of the CL in two ways. First, they can act as electrocatalysts or inhibitors of reactions (7)–(10), and thus change the stoichiometric coefficient via these reactions. It has been established that antimony increases the rate of reaction (8) and inhibits reaction (9) [9]. Tin catalyzes both reactions (8) and (9) [15]. Consequently, the integral stoichiometric coefficient of the CL for alloys containing one or both additives is higher. Table 3 illustrates the influence of antimony, arsenic and silver on the integral stoichiometric coefficient of the CL formed on galvanostatic oxidation of lead electrodes containing the above additives with a current of 6 mA cm^{-2}. Arsenic and silver maintain a stoichiometric coefficient close to the critical zone of lead oxide conductivities.

Table 3
Influence of alloy additive on the integral stoichiometric coefficient of the CL

Additive	n in the CL	Ref.
Sb	$PbO_{1.70-1.85}$	[16]
As	$PbO_{1.40-1.65}$	[17]
Ag	$PbO_{1.50-1.60}$	[17]

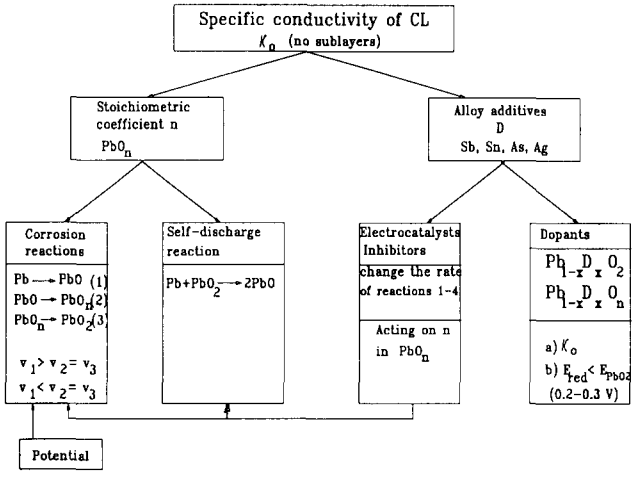

Fig. 7. Parameters that determine the specific conductivity of the CL.

The second influence of alloying additives is to alter the semi-conductor properties of the oxides in the CL. The ions of the alloying additives are incorporated into the structure of PbO_2 or PbO_n and form mixed oxides of the type $Pb_{1-x}D_xO_2$ and/or $Pb_{1-x}D_xO_n$. As a result of this the concentration of charge carriers and/or their mobility can be increased/decreased and this leads to an increase/decrease in specific conductivity of the oxides κ_0. This feature will shift the κ_0/n curve toward a higher/lower stoichiometric coefficient. On the other hand, during discharge, mixed oxides can be reduced at more negative potentials than that of PAM reduction. In this case, the CL will remain highly conductive while the major part of the PAM will be reduced and, hence, the plate potential will be determined by the processes in the PAM.

It has been established that on anodic polarization of Pb–Sb [18], Pb–Sn [1] and Pb–As [1] electrodes, mixed lead dioxides of the type $Pb_{1-x}D_xO_2$ are formed (D stands for the dopant, Sb, Sn or As). The mixed dioxides are reduced at potentials between 0.2 and 0.3 V more negative than the potential of PbO_2 reduction. A general scheme of the relationships between the above parameters, on which the specific conductivity of the CL depends, is presented in Fig. 7.

3.3. Passivation of the positive plate (PPP)

Passivation of the positive plates (PPP) occurs when a separate PbO layer with a certain thickness is formed in the CL. This layer creates a high resistance in the electrical circuit of the charged positive plate. Hence, discharge of the plate starts at potentials between 0.5 and 1.2 V more negative than the equilibrium potential of the $PbO_2/PbSO_4$ electrode. PPP can occur via the following reactions.

(i) Anodic corrosion at potentials 1.2–1.3 V versus Hg/Hg_2SO_4 electrode due to diffusion of oxygen through the corrosion layer [19]:

$$Pb + O \longrightarrow PbO \quad (11)$$

This reaction results in the formation of the electrode system $Pb/PbO/PbO_2$.

(ii) Self-discharge of the positive plate at open circuit:

$$Pb + PbO_2 \longrightarrow 2PbO \quad (12)$$

This process takes place during the drying of formed plates at high temperature (thermopassivation) [20] or during long battery storage (storage passivation) [21]. Here, again, the electrode system $Pb/PbO/PbO_2$ is formed as a result.

Passivation of the positive plate can be strongly hampered by dopants. It has been established that tin increases the conductivity of the PbO layer (tin-free effect, [15,22,23]). Moreover, passivated electrodes can be depassivated by: (i) PbO layer reduction to Pb by cathodic polarization [23]; (ii) PbO layer oxidation by O_2 on overcharge of the positive plate. Oxygen diffuses into the corrosion layer reaching the PbO layer and oxidizing it to a higher valency, low-resistance oxide [20].

PPP should not be directly related to the absence of antimony or dopants, and has to be distinguished from the phenomena that cause the PCL effect.

3.4. Area of the CL surface through which current flows between the grid and PAM

The area through which current flows in the CL is expressed by the equation:

$$S_{CL} = S_{grid} - S_{cracks} - \Delta S_{PBO_2} \quad (13)$$

where S_{cracks} represents the area of the cracks at a given thickness of the CL through which the current cannot pass. ΔS_{PbO_2} is the fraction of the CL surface on which PbO_2 has been reduced during discharge. It is a function of the time of discharge.

Cracks in the CL are formed as a result of internal stresses accumulated in the CL during oxidation of Pb to PbO_2. The molar volume of PbO_2 is 38% greater than that of Pb [24] and oxidation reactions occur in

the solid state. This creates internal stresses. On increase of the CL thickness, these stresses grow until the moment is reached at which they are liberated and cause the CL to crack. This process may occur in the bulk of the CL and/or at the boundaries of the CL/PAM, thus an effective S_{cracks} area should be accounted for.

Cracks can also result from non-uniform heating of the CL (thermal loop, see above).

It has been established that both the CL and the PAM contain gel zones [6,9]. The latter represent an elastic element in their structure (Fig. 5). This enables part of the stresses to be released through displacement of these zones without cracking of the CL. Thus, gel zones play the role of 'hinges' and maintain a low value of S_{cracks}. It has been established that the PAM is 30–35% hydrated [10]. The degree of hydration of the CL formed on pure lead electrodes is about 10% [8], whereas on Pb–Sb and Pb–Sn electrodes hydration of the CL varies with the contents of antimony and tin in the alloy [2,9]. These dependencies are presented in Table 4. It can be seen that tin exerts a stronger influence on PbO_2 hydration than antimony.

The hydration of PbO_2 affects its mechanical properties. It has been established that the hardness of the CL obtained on Pb–4wt.%Sb grids is 54 kg mm^{-2} against 88 kg mm^{-2} for Pb–0.09wt.%Ca grids [25]. Obviously, the antimonial CL is more elastic due to the higher content of gel zones in it. This makes it less susceptible to cracking.

During discharge and self-discharge, part of the PbO_2 in the CL is reduced to $PbSO_4$ which is an insulator. Consequently, the area through which the current flows is reduced by ΔS_{PbO_2}, which in turn affects the electrode polarization. This occurs usually at the end of discharge if the plate capacity is determined by the electronic conductivity of the grid/PAM interface.

3.5. Thickness of the corrosion layer

Formation of the CL starts during manufacture of the positive plate and it continues to grow during battery operation. Grid alloys are oxidized faster at higher temperatures in the presence of humidity and oxygen. Such conditions are established during curing of the plates. It has been found that if curing is carried out at elevated temperatures (80 °C), the PbO obtained ensures good adhesion between grid and PAM [26,27]. During formation, PbO is oxidized to PbO_2 and the CL reaches a certain thickness, l_0.

Table 4
Influence of antimony and tin content in the alloy on the degree of hydration of PbO_2 [1,9]

Sb (wt.%)	Hydration (%)	Sn (wt.%)	Hydration (%)
1.0	16	0.05	10.04
3.0	18	0.1	16.23
5.0	22	0.5	24.20

During battery operation, the thickness of the CL increases due to oxygen diffusion through the layer and step-by-step oxidation of Pb to PbO, PbO_n and PbO_2 (reactions (7)–(9)) [28]. The thickness of the CL grows by $\Delta l_{0p}(Z)$ on increasing the number of cycles Z until the overall thickness reaches a constant value, l_{st}, i.e.,

$$l = l_0 + \Delta l_{0p}(Z) \longrightarrow l_{st} \quad (14)$$

This value is determined by the balance between the rates of lead oxidation and of transformation of the CL into the PAM. This balance is reached within 20–30 cycles. The stationary thickness, l_{st}, has different values in the various parts of the grid surface and thus an effective thickness is achieved.

4. Active-mass collecting layer (AMCL)

The main function of the active-mass collecting layer is to collect the current from the capacity-bearing part of the PAM. The CL/AMCL interface is not very clearly identified when the porous corrosion sub-layer is formed. Both layers are porous; they are similar in character but differ by origin. At the beginning of battery cycling, the porous sub-layer is not yet formed and the AMCL is in direct contact with the continuous sublayer. This case will be discussed later.

4.1. Specific resistivity of the AMCL

This depends on the structure of the PAM. The AMCL consists of a continuous skeleton and a system of pores [29]. The skeleton contains crystal zones (α- and β-PbO_2) with dimensions of the order of 300–700 Å and hydrated ($PbO(OH)_2$) gel-like zones [6]. Crystal zones have the properties of degenerated semi-conductors with specific conductivities presented in Table 1. Gel zones consist of hydrated polymer chains that exhibit both electronic and protonic conductivity and inter-connecting the crystal zones. The whole PAM skeleton (including AMCL + capacity-bearing PAM) represents an integral electronically conductive system.

On oxidation, the allowing additives are incorporated into the CL When they get in contact with the solution in the pores, they are dissolved in it. After that, they are absorbed into the hydrated zones of the PAM and are thus incorporated into the structure of the skeleton [30]. Alloying additives influence the properties of the PAM in two ways, namely: (i) by changing the conductivity of the gel and crystal zones; (ii) by altering the ratio between gel and crystal zones [30]. Alloying

additives that exhibit the strongest impact are, antimony tin, arsenic, etc.

4.2. Effect of the type of PAM skeleton on the properties of the CL/PAM interface

Fig. 8 presents a scheme of the CL/PAM interface for two different PAM skeletons before the porous sub-layer of the CL has been formed. The first skeleton is built of thin branches, and the second one comprises thick branches. Very often the PAM obtained from tribasic lead sulfate (3BS) pastes features a skeleton of the first type, while that formed from tetrabasic lead sulfate (4BS) pastes has the second type of skeleton.

During discharge, part of the PbO_2 in the collecting layer is reduced and the cross section of the skeleton branches decreases. Their resistance increases. During this process, a critical area of the cross section is reached and yields such a high resistance that no current actually flows through this branch of the system. If the branches have small cross sections, this critical area is reached much earlier than for a skeleton with thicker branches. Often discharge does not lead to full reduction of the PbO_2 branches. Most of them become thinner at the end of discharge. Hence, the skeleton structure affects the capacity of the plate. This conclusion is supported by the following experimental results.

The PAM skeleton structure depends on the type of basic lead sulfates in the initial paste. These sulfates are oxidized to PbO_2 through metasomatic processes. Fig. 9 presents the capacity curves on cycling of positive plates prepared using three different types of pastes [31]. The PAM obtained from monobasic lead sulfate (1BS) pastes has a skeleton with thin branches and exhibits high initial capacity, but short cycle life. Plates prepared with 3BS pastes have a PAM skeleton built of agglomerates sized between 2 and 3 μm. Such plates have a longer cycle life. Crystals of 4BS have dimensions between 10 and 50 μm and the PAM skeleton obtained as a result of their oxidation features thicker branches. Consequently, this type of plate exhibits the longest cycle life. It can be expected that the structure of the PAM skeleton would exert its influence on the discharge parameters most strongly through the CL/AMCL interface.

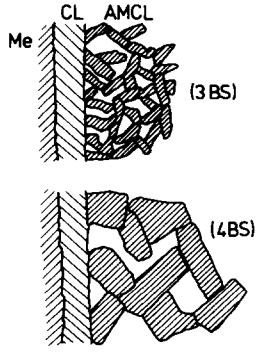

Fig. 8. A model for the CL/PAM interface. PAM skeleton is built of two types of agglomerates.

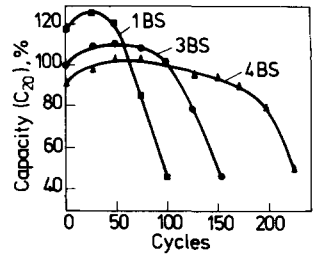

Fig. 9. Dependence of plate capacity on the number of cycles for positive plates prepared with 1BS, 3BS and 4BS pastes that yield three different types of PAM skeleton.

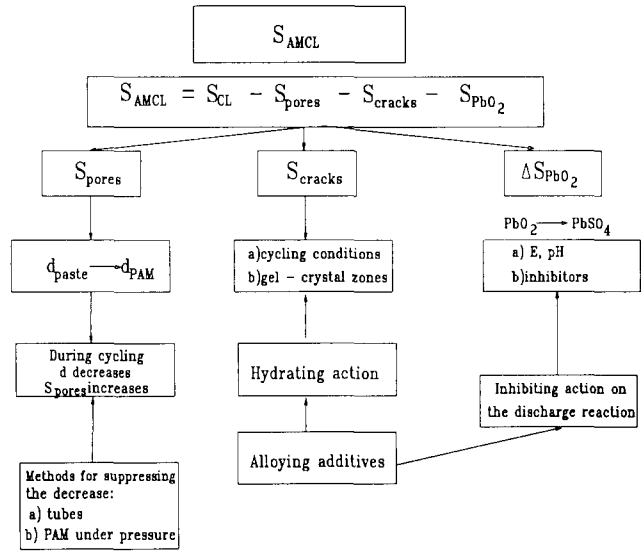

Fig. 10. Parameters influencing the effective area through which current flows in the AMCL layer.

4.3. Effective surface area of the AMCL through which the current is transferred between PAM and grid

Consider the surface area of the interface CL/AMCL. The effective area through which electronic current flows is given by the following equation

$$S_{AMCL} = S_{CL} - S_{pores} - S_{cracks} - \Delta S_{PbO_2} \quad (15)$$

S_{CL} is the area of the continuous CL. Examine the case when a porous sub-layer is not yet formed (Fig. 8). The influence of the technological parameters on the separate terms in Eq. (15) is presented schematically in Fig. 10.

S_{pores} is the area of the CL/electrolyte interface in the pores. It depends on the PAM density and is determined technologically by the paste density. Upon cycling, the density of PAM decreases. It can be expected that the cross section of the skeleton branches in the

AMCL will be reduced. This may exclude parts of the AMCL branches from current collection and transfer. One of the reasons for the decrease in density of the collecting layer during cycling is the pulsation of the PAM during charge and discharge. Takahashi et al. [32] have established that when the active block (containing plates with Pb–Sn–Ca grids) is assembled under pressure, the plates increase their thickness, but only very slightly. Concomitantly, the ohmic resistance increases slowly and the plates have high capacity and long cycle life. Batteries with plates assembled under a pressure of 0.4 kg cm^{-2} exhibit a life that is twice that of batteries whose active block is under a pressure of 0.2 kg cm^{-2}. When the CL cracks, the two opposite surfaces of the cracks may remain in electrical contact under the action of the pressure applied. Through this method, however, the separator is subjected to extra load. The plates may get short-circuited through the separator, which would limit the life of the battery. This method has found application in small-sized batteries. The second method for limiting the pulsation of the plates on cycling is through enclosing the active mass in porous tubes and thus limiting its volume. With this method, short-circuiting of the plates is avoided. The method has found application in the manufacture of high-power batteries.

S_{cracks} is the surface area of the cracks at the CL/AMCL interface or in the AMC layer itself. The cracks are caused by internal stresses that appear during discharge due to the difference in molar volumes of PbO_2 and $PbSO_4$. $PbSO_4$ has a 92% greater molar volume than PbO_2 [24]. The degree of cracking of the AMCL skeleton depends on its gel content which, in turn, is influenced by the type and amount of alloying additives.

ΔS_{PbO_2} is the area subtracted from the cross section of PbO_2 skeleton branches of the AMCL by its reduction to $PbSO_4$ during discharge. As discharge advances, this area increases. The process continues until a critical value of the cross-sectional area of most of the branches is reached and the current flow through them is strongly impeded.

The discharge reaction $PbO_2 \rightarrow PbSO_4$ is influenced by the potential of the plate (electrode polarization), the pH of the solution in the pores of the AMCL, and the inhibitors. Alloying additives could exert an inhibiting action on the above reaction.

Returning to the example given above (i.e., 50 cm^2 grid area), a rough estimate of the effective area of the CL/AMCL interface can be made. At PAM porosity of 50%, S_{pores} will amount to about 25 cm^2. If we assume that S_{cracks} is about 30%, then the area $S_{AMCL/CL}$ through which current flows at the beginning of discharge is of the order of 16 cm^2/plate. If a PAM utilization of 50% is accepted, then at the end of discharge, the area of the CL/AMCL interface through which current flows is of the order of 8–10 cm^2. This is a value close to the critical one for both the interface thermal loop and for its susceptibility to changes in the oxide stoichiometric coefficient due to discharge reactions. The specific resistivity of CL and AMCL is changed. This relation depends strongly on dopants. The relationship is illustrated by experimental data in Fig. 2, where its influence on the contact resistance and, through it, on the plate capacity is shown.

The above rough estimates indicate that the *CL/AMCL interface is the most critical zone in the positive plate*. In this zone, the influence of the different parameters is exerted most strongly. This is presented as the general scheme in Appendix C.

4.4. Effective thickness of the AMCL

The effective thickness of the AMCL is determined by the thickness of the PAM layer when functioning as a current collector from the capacity-bearing part of the PAM. This layer does not undergo essential changes during cycling.

5. Experimental verification of the above theory of the phenomena that occur at the grid/PAM interface

The theoretical principles of battery design and manufacture proposed above have been applied for building experimental cells and batteries. These experimental measurements have been performed together with G. Papazov. The financial support provided by ILZRO, the International Lead Zinc Research Organization, Inc., for this experimental work is gratefully acknowledged [1].

5.1. Positive-plate design

In order to increase the coefficient of PAM utilization and to decrease the current density at the grid/PAM interface, the values of γ were chosen between 0.5 and 0.8 g PAM per 1 cm^2 of grid surface. In order to ensure a uniform current density throughout the whole surface area of the collector, the latter was shaped as straps connected into a comb-like grid. The straps were coated with a uniform PAM layer. The positive plate design is given in Fig. 11. In order to slow down the decrease in PAM density during cycling, the latter was encapsulated in flat polyester woven tubes produced by Incotex Ltd., Bulgaria and Tergar Co. Italy. Table 5 gives a summary of some of the technical parameters of the experimental tubular plates.

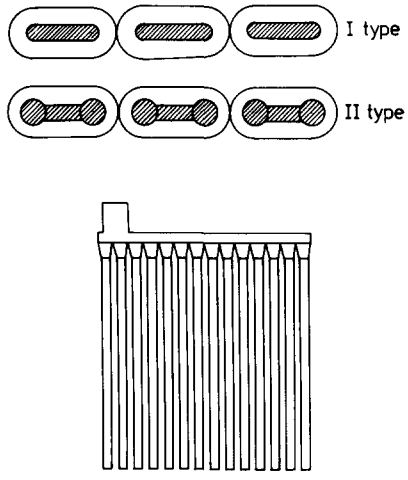

Fig. 11. Cross section of: (a) tubular electrodes; (b) spine grids.

Table 5
Technical parameters of the newly designed, flat tubular plates

Plate thickness (mm)	4.0
Plate height (mm)	160
Width of flat spine (mm)	6.0
Thickness of flat spine (mm)	1.2
Thickness of PAM round the spine (mm)	1.4
γ-Coefficient (g PAM/cm^2 spine surface)	
Type I	0.79
Type II	0.56

5.2. Technology for manufacture of flat tubular plates

5.2.1. Grid alloy additives

Antimony, tin and arsenic were chosen due to their well-known effect as dopants and their hydrating action on PAM, as well as because of their electrocatalytic effect on the oxidation of PbO to PbO_2. Flat 'combs' of straps were cast from the following alloys: Pb–1.8wt.%Sb–0.15wt.%As and Pb–0.6wt.%Sn–0.08wt.%Ca.

5.2.2. Active mass

In order to obtain a strong and resistant PAM skeleton with thick branches, 4BS pastes were used. The tubes were filled with a water suspension of 4BS paste. The paste was prepared using leady oxide and H_2SO_4 (1.4 sp. gr.) at an H_2SO_4/PbO ratio equal to 6%. The temperature of paste preparation was 90 °C and time of paste mixing was 40 min. Under these conditions, 4BS crystals sized between 15 and 20 μm are formed. The tubes were filled with the suspension using a specially designed filling device. In order to achieve pores with small cross section in the AMCL, PAM with a density of 4.6 g cm^{-3} was prepared.

The tubular electrodes were subjected to curing at 85 °C in a chamber. At this temperature, the CL ensures good connection between the grid and the PAM. X-ray analyses showed that the cured paste contained 4BS, αPbO and less than 1 wt.% of unreacted Pb. From SEM observations of the structure of the cured paste, the average size of the 4BS crystals was determined to be 20–30 μm. The plates were formed in H_2SO_4 (1.15 sp. gr.) by passing 520 Ah for the formation of 1 kg of active mass.

5.3. Results from testing of cells with flat tubular electrodes

5.3.1. Capacity tests

The cells consisted of one tubular plate or a single-tube electrode placed between two SLI negative plates. Thus, the cell capacity was determined only by the positive electrode. The cells were flooded with H_2SO_4 (1.28 sp. gr.) and subjected to successive capacity tests, Peukert dependence measurements, and cycle-life tests. The rated capacity was calculated at 50% utilization of the active mass. The cells were tested at the 5 h rate of discharge. Fig. 12 presents the discharge curves obtained for electrodes with the two types of spine profiles (Fig. 11) at 25 °C [1].

The electrodes with type-II spines exhibit a discharge voltage that is higher by about 10–15 mV than that of the cells with type-I spines.

Within the first three cycles, all cells reached capacities between 105 and 113% of the rated values.

5.3.2. Peukert dependence ('banana' curve)

Fig. 13 presents the specific capacity versus discharge current per 1 kg PAM. The data refer to single-tube electrodes (CLEPS-SE, Pb–Ca–Sn alloy) and whole plates (CLEPS-TP, Pb–Sb–As alloy). For comparison, the 'banana curves' for commercial SLI and electric-vehicle (EV) positive plates are also given.

At the 5 h rate of discharge, flat tubular plates exhibit a specific capacity of 142 Ah kg^{-1} (64% utilization of PAM) against 124 Ah kg^{-1} for SLI plates and 62 Ah kg^{-1} for EV plates. At discharge current densities of up to 50 A kg^{-1} PAM (a range of current densities within which the battery is actually used as a source

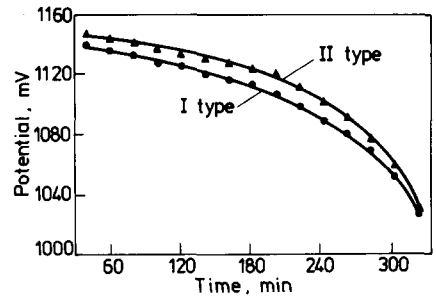

Fig. 12. Discharge curves at 5 h rate of discharge.

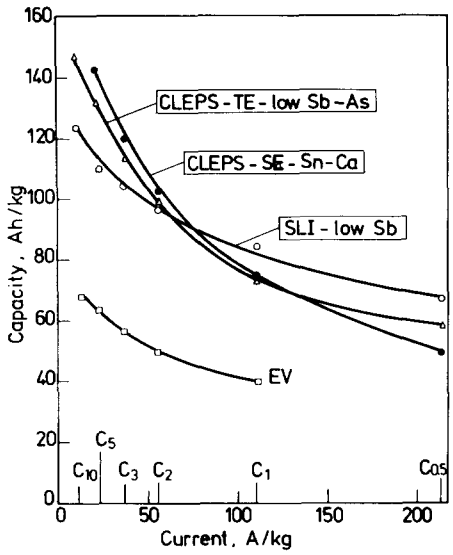

Fig. 13. Specific capacity vs. discharge current for the newly designed single-tube electrodes (CLEPS-SE) and for tubular plates (CLEPS-TP), as well as for commercial SLI and EV positive plates.

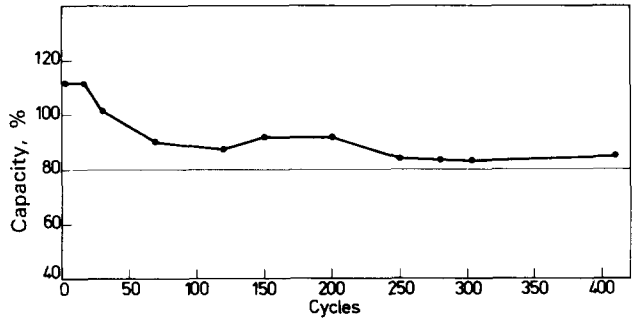

Fig. 14. Dependence of the capacity of single-tube electrodes on the number of cycles. Cycling tests are ongoing.

of energy in electric vehicles), flat tubular plates have higher capacity than that of SLI grid plates. The proposed, new, flat tubular electrode design with reduced PAM weight per 1 cm^2 of spine surface, when combined with an appropriate PAM structure obtained from 4BS pastes, ensure high specific capacity at a given current density.

5.3.3. Cycle life tests

Fig. 14 presents the capacity as a function of the number of cycles for single tube electrodes with Pb–Sn–Ca spines. Each cycle comprised 5 h charge with a current density of 13 mA/g PAM and 1 h discharge with a current density of 56 mA/g PAM. Cycling was performed at 70% DOD and 35% utilization of the active mass at 1 h discharge rate. The cells have completed 410 cycles up to now and the cycling tests are ongoing. On receipt of the proofs the cells had reached end of life after 725 cycles because of strap corrosion. Recently, batteries with flat tubular plates have been subjected to testing.

Bearing in mind that the straps were made from Pb–Sn–Ca alloys and subjected to the above hard cycling duty, the cycle life reached is an encouraging result, which supports the above theory and the proposed new design and manufacturing technology for positive-plate production.

The testing results indicate that plates with low Sb or Sb-free grids that are susceptible to the phenomena causing PCL, need a new production technology and new principles of plate design. In the present work, the basic principles of this new technological and design approach are elaborated. These are aimed at improving the cycle life of the above-mentioned type of batteries.

Appendix A

A general scheme presenting the inter-relations between η (coefficient of active mass utilization), Z (cycle life) and γ parameter (g PAM/cm^2 current collector) is presented in Fig. A1 in a three-coordinate system. The conditions of deep cycle-life testing are constant. The function passes through a maximum.

When $\gamma > \gamma_m$ then $\eta < \eta_m$. The cycle life of the positive plates decreases as at the grid/PAM interface problems appear (PCL effect).

When $\gamma < \gamma_m$ then $\eta > \eta_m$. The cycle life of the positive plates decreases as PAM problems appear (softening and shedding of the active mass).

The values of Z_m, η_m, and γ_m depend on the design of the plates and the technology of its manufacturing. In this paper, are presented the parameters that influence the positive plate cycle-life when $\gamma > \gamma_m$.

Appendix B

During solid-state oxidation of lead by oxygen, α-PbO is formed. A semi-conductor mechanism of the

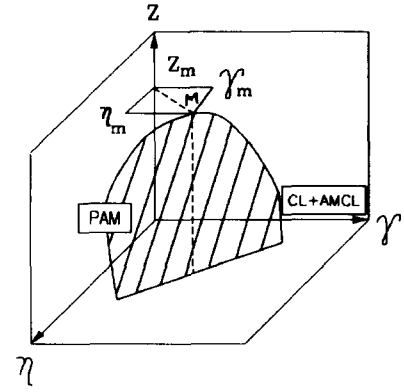

Fig. A1. General scheme of the relations between coefficient of active mass utilization η on γ-parameter and cycle life Z.

oxidation of PbO to PbO_2 was proposed in Ref. [33]. α-PbO contains in its crystal lattice empty layers with a thickness of 2.76 Å [34]. Oxygen atoms have a diameter of 1.32 Å. This allows them to intercalate freely into the empty layers of the α-PbO crystal lattice. As a result of this, a certain oxygen concentration N_O is maintained in the oxide depending on the partial oxygen pressure at the oxide/solution interface. Oxygen atoms are strong acceptors of electrons. They oxidize Pb^{2+} to Pb^{3+} and a non-stoichiometric PbO_n oxide is formed ($1 < n < 1.5$). This change in stoichiometric coefficient is not associated with alteration of the crystal lattice, only the concentration of defects N_O increases. When n reaches a value of 1.5, the concentration of defects in the lattice becomes so high that the lattice is restructured into an α-PbO_2 one.

The trivalent Pb^{3+} ions in the crystal lattice of PbO_n accept and release electrons readily, and thus create a p-type conductivity (hole conductivity). [35]. Upon increase of the Pb^{3+} concentration, both the stoichiometric coefficient and the concentration of holes rise and the conductivity is increased (Fig. 6) [33]. The presence of foreign ions (dopants) in the oxide influences this dependence.

Appendix C

Fig. C1 represents a general scheme of the changes in the area through which current passes in the CL, AMCL and PAM with the distance from the current collector (hatched region).

The area through which the current passes in the CL decreases from the cracks. At the CL/AMCL interface, it decreases sharply as the pore surface is developed at this interface. In the AMCL layer, it decreases from the cracks that are formed in this layer. The area through which current passes in the PAM increases sharply. The specific resistivity changes with the distance from the current collector, as the phase composition at the interface is changed.

During discharge S_{ca} in the AMCL decreases as a part of PbO_2 is reduced and the resistance of the grid/PAM interface increases. The curve moves down with state-of-discharge.

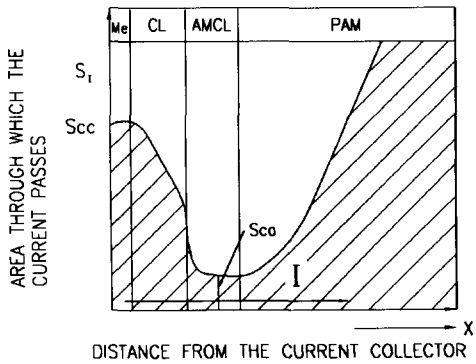

Fig. C1. General scheme of the changes in cross-sectional area parallel to the current-collector surface through which current passes with the distance from the current collector (hatched region).

References

[1] D. Pavlov, G. Papazov, M. Bojinov and B. Monahov, *Advanced Lead–Acid Battery Consortium (ALABC) Project AMC-004, Annual Rep.*, ILZRO, Research Triangle Park, NC, USA, 1994.
[2] A.F. Hollenkamp, K.K. Constanti, M.J. Koop, L. Apateanu, M. Calabek and K. Micka, *J. Power Sources, 48* (1994) 195–215.
[3] W. Mindt, *J. Electrochem. Soc., 116* (1969) 1076–1080.
[4] V.I. Perelman, *A Comprehensive Chemist's Handbook*, Scientific and Technical Publishers, Moscow, 1954, p. 237 (in Russian).
[5] D. Pavlov, *J. Power Sources, 48* (1994) 179–193.
[6] D. Pavlov, *J. Electrochem. Soc., 139* (1992) 3075–3080.
[7] D. Pavlov, *J. Power Sources, 46* (1993) 171–190.
[8] B. Monahov and D. Pavlov, *J. Appl. Electrochem., 23* (1993) 1244–1250.
[9] B. Monahov and D. Pavlov, *J. Electrochem. Soc., 141* (1994) 2316–2326.
[10] D. Pavlov, I. Balkanov, T. Halachev and P. Rachev, *J. Electrochem. Soc., 136* (1989) 3189.
[11] D.L. Douglas and G.M. Mao, in D.H. Collins (ed.), *Power Sources 4*, Oriel, Newcastle-upon-Tyne, 1973, pp. 561–567.
[12] B.K. Mahato, *J. Electrochem. Soc., 126* (1979) 365–370.
[13] D.A.J. Rand, *J. Power Sources, 23* (1988) 257–277.
[14] F. Lappe, *J. Phys. Chem. Solids, 23* (1962) 1563–1572.
[15] D. Pavlov, B. Manahov, M. Maja and N. Penazzi, *J. Electrochem. Soc., 136* (1989) 27–34.
[16] T. Rogachev, *J. Power Sources, 23* (1988) 331–340.
[17] D. Pavlov and T. Rogachev, *Electrochim. Acta, 31* (1986) 241–252.
[18] D. Pavlov, B. Monahov, G. Sundholm and T. Laitinen, *J. Electroanal. Chem., 305* (1990) 57–70.
[19] K.R. Bullock and M.A. Butler, *J. Electrochem. Soc., 133* (1986) 1085–1091.
[20] D. Pavlov and S. Ruevski, *J. Electrochem. Soc., 126* (1979) 1100.
[21] J. Garche, N. Anastasijevic and K. Wiesener, *Electrochim. Acta, 26* (1981) 1363–1373.
[22] H.K. Giess, in K.R. Bullock and D. Pavlov, (eds.), *Advances in Lead–Acid Batteries*, Vol. 84-14, The Electrochemical Society Inc., Pennington, NJ, USA, 1984, pp. 241–251.
[23] R.F. Nelson and D.M. Wilson, *J. Power Sources, 33* (1991) 165–185.
[24] H. Bode, in J. Brodd and K. Kordesch (eds.), *Lead–Acid Batteries*, Wiley, New York, 1977, p. 13, Table 2.4.
[25] S. Hattori, M. Yamamura, M. Kono, M. Yamane, H. Nakashito, J. Yamashita and J. Nakayama, *ILZRO Project LE-276, Rep. No. 5*, ILZRO, Research Triangle Park, NC, USA, 1980.
[26] D.A.J. Rand and L.T. Lam, *The Battery Man*, (Nov.) (1992) 19.
[27] D. Pavlov, S. Ruevski and T. Rogachev, *Annual Rep.*, CLEPS, Bulgarian Academy of Sciences, Sofia, Bulgaria, 1993.
[28] D. Pavlov and T. Rogatchev, *Electrochim. Acta, 23* (1978) 1237–1246.
[29] D. Pavlov and E. Bashtavelova, *J. Electrochem. Soc., 131* (1984) 1468–1473.

[30] D. Pavlov and I. Balkanov, *J. Electrochem. Soc., 139* (1992) 1830–1835.
[31] G. Papazov and D. Pavlov, *Annual Rep.*, CLEPS, Bulgarian Academy of Sciences, Sofia, Bulgaria, 1975; D. Pavlov, in B.D. McNicol and D.A.J. Rand (eds.), *Power Sources for Electric Vehicles*, Elsevier, Amsterdam, 1984, p. 344.
[32] K. Takahashi, M. Tsubota, K. Yonezu and K. Ando, *J. Electrochem. Soc., 130* (1983) 2144–2149.
[33] D. Pavlov, *J. Electroanal. Chem., 118* (1978) 845.
[34] J.S. Anderson and M. Sterns, *J. Inorg. Nucl. Chem., 11* (1959) 272.
[35] L. Hejne, *J. Phys. Solids, 22* (1961) 207.